Available online at www.sciencedirect.com
SCIENCE DIRECT®
Journal of Sound and Vibration 287 (2005) 707–722
JOURNAL OF SOUND AND VIBRATION
www.elsevier.com/locate/jsvi

Damage size estimation by the continuous wavelet ridge analysis of dispersive bending waves in a beam

Ik Kyu Kim, Yoon Young Kim*

Multiscale Design Center, School of Mechanical and Aerospace Engineering, Seoul National University, Shinlim-Dong San 56-1, Kwanak-Gu, Seoul 151-742, Republic of Korea

Received 15 December 2003; received in revised form 22 November 2004; accepted 29 November 2004
Available online 16 February 2005

Abstract

The damage assessment in a structure consists of the estimation of its location and extent. The objective of this work is to assess the damage size using the ratio of the incident wave toward and the reflected wave from the damage. Since waves to be analyzed are of the bending type, the measured signals are highly dispersive; it is almost impossible to estimate the magnitude ratio alone in the time domain. So, we propose to use the continuous wavelet transform of the measured signal and perform the ridge analysis in order to extract accurately the magnitudes of the incident and the reflected waves for a range of frequencies of interest from the measured wave signal. Wave experiments are conduced in a slender cylindrical beam and the magnetostrictive sensors are used to capture the bending waves in the beam. To correlate the magnitude ratio with the damage size, we employ the Timoshenko beam theory. Several experiments are conducted to check the effectiveness of the proposed wavelet-based method.

1. Introduction

The damage estimation problem has been a popular subject for various reasons [1–3]. In this work, we will be mainly concerned with the damage size estimation using guided bending waves propagating in a long cylindrical beam. Though common damage detection methods using guided

*Corresponding author. Tel.: +82 2 880 7154; fax: +82 2 883 1513.
E-mail address: yykim@snu.ac.kr (Y.Y. Kim).

0022-460X/$ - see front matter © 2005 Elsevier Ltd. All rights reserved.
doi:10.1016/j.jsv.2004.11.033

waves are usually based on longitudinal or torsional waves as they are less dispersive, there are some situations where bending waves are primary energy carriers. Quite often, bending waves in addition to longitudinal waves are reflected from a crack even if only longitudinal waves are incident. In this case, the additional analysis of bending waves will definitely enhance the accuracy of damage estimation.

Our goal in this work is to correlate the damage size and the ratio of the bending wave reflected from and the incident wave into a crack, where the ratio is estimated by the continuous wavelet transform of the measured signal. The continuous wavelet transform [4] has been successfully used in various applications [5–10] including the damping identification [5] and damage detection [9].

As far as the CWT application in damage detection is concerned, CWT has been mainly used for damage location estimation, not for damage size estimation. In this work, the ridge in the wavelet-transformed time–frequency plane is traced to compare the magnitude of the incident wave and the magnitude of the reflected wave from a crack. The ridge method has been used and developed in other applications [5], but not in damage size assessment. For damage size assessment, a theoretical foundation to correlate the damage size and the magnitude of reflected wave from a crack must be provided. In this work, the CWT-based ridge method will be applied in the damage detection of a beam, so the one-dimensional Timoshenko beam theory is employed [11–13]. Although, the use of the three-dimensional elasticity equations improves the accuracy of the prediction, they are too complicated to use. Even with the simpler Timoshenko equation, the potential of the CWT-based wavelet ridge method may be effectively demonstrated.

For wave signal acquisition, magnetostrictive sensors [14–21] were used. The effectiveness of the magnetostrictive sensor application for bending wave measurement may be found in Kim et al. [19] and Lee and Kim [21].

2. Mechanics of bending waves in a beam

In this section, we will briefly explain the mechanics involved in the propagation and reflection of elastic bending waves in a beam. Assuming that the beam is slender, we may use the Timoshenko beam theory [11] for simplified, yet quite satisfactory analysis.

Fig. 1 illustrates analysis models: a beam with a partial non-symmetric crack and a beam with a symmetric circumferential crack. Fig. 1 schematically shows incident, reflected and transmitted waves near a crack. The crack is designated by a small undercut lying between $x = 0$ and $x = d$. In Fig. 1, the symbol A_1 denotes the incident bending wave toward the crack. The symbols A_2 and A_3 represent the traveling waves to the right, and the symbols B_2 and B_3 represent the evanescent waves to the right. The symbols C and D denote the propagating and evanescent parts of the reflected waves to the left, respectively.

In the Timoshenko beam theory, the displacement w and the rotation θ of the surface normal are the field variables, which are illustrated in Fig. 2. The rotation of the middle plane is given by $\mathrm{d}w/\mathrm{d}x$. In the Timoshenko beam theory, the shear strain, which is given by $\gamma = \mathrm{d}w/\mathrm{d}x - \theta$, is taken into account. To analyze the wave reflection and transmission in the problem shown in

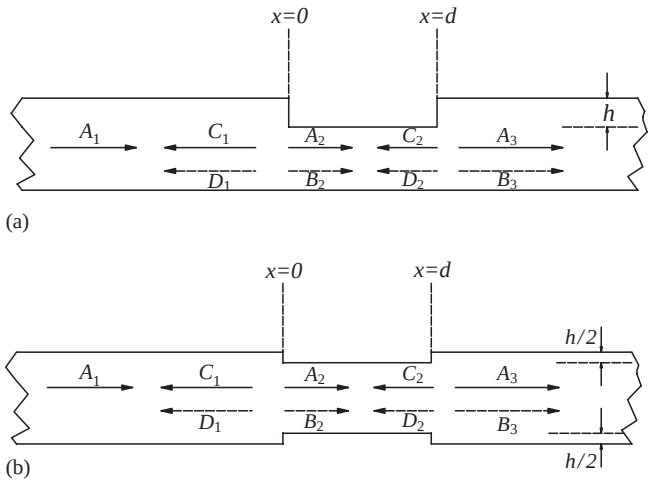

Fig. 1. One-dimensional model for incident, reflected and transmitted waves in a beam having a crack of length d and depth h: (a) with partial crack, (b) with circumferential crack.

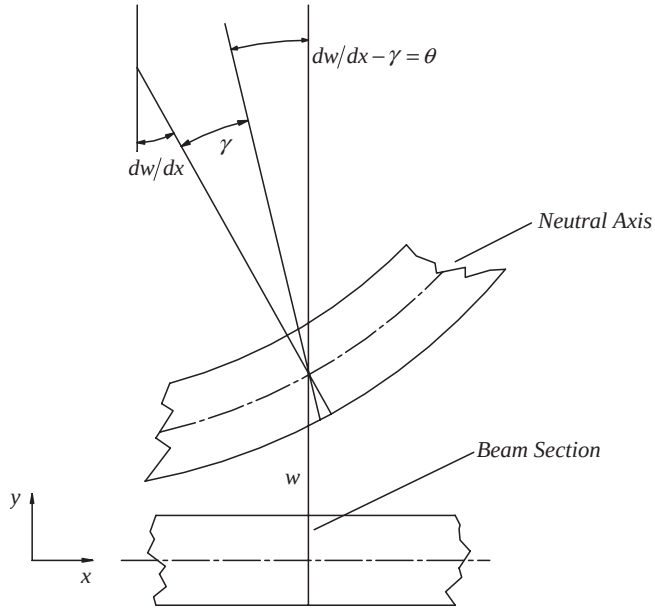

Fig. 2. The kinematics of the Timoshenko beam theory.

Fig. 1, the following form of solution can be used (see, e.g., Doyle [12]):

$$w_1(x,t) = (A_1 e^{-ik_1 x} + C_1 e^{ik_1 x} + D_1 e^{k_1 x}) e^{i\omega t},$$
$$w_2(x,t) = (A_2 e^{-ik_2 x} + B_2 e^{-k_2 x} + C_2 e^{ik_2 x} + D_2 e^{k_2 x}) e^{i\omega t},$$
$$w_3(x,t) = (A_3 e^{-ik_3 x} + B_3 e^{-k_3 x}) e^{i\omega t}, \quad (1a)$$

$$\theta_1(x,t) = (\bar{A}_1 e^{-ik_1 x} + \bar{C}_1 e^{ik_1 x} + \bar{D}_1 e^{k_1 x}) e^{i\omega t},$$
$$\theta_2(x,t) = (\bar{A}_2 e^{-ik_2 x} + \bar{B}_2 e^{-k_2 x} + \bar{C}_2 e^{ik_2 x} + \bar{D}_2 e^{k_2 x}) e^{i\omega t},$$
$$\theta_3(x,t) = (\bar{A}_3 e^{-ik_3 x} + \bar{B}_3 e^{-k_3 x}) e^{i\omega t}. \tag{1b}$$

In Eq. (1), w_1 and θ_1 denote the field variables in the beam on the left of the crack, and w_2, θ_2, in the crack section and w_3, θ_3, in the beam on the right of the crack. The wavenumber is denoted by k and the angular frequency, by ω. The relation between the wavenumber k and frequency ω is

$$k = k_L(\omega) \quad \text{or} \quad k_H(\omega),$$

where

$$k_L^2(\omega) = \frac{1}{2}\left[\left(\frac{1}{c_s}\right)^2 + \left(\frac{1}{c_b}\right)^2\right]\omega^2 + \left[\left(\frac{\omega}{c_b q}\right)^2 + \frac{1}{4}\left\{\left(\frac{1}{c_s}\right)^2 - \left(\frac{1}{c_b}\right)^2\right\}^2 \omega^4\right]^{1/2}, \tag{2a}$$

$$k_H^2(\omega) = \frac{1}{2}\left[\left(\frac{1}{c_s}\right)^2 + \left(\frac{1}{c_b}\right)^2\right]\omega^2 - \left[\left(\frac{\omega}{c_b q}\right)^2 + \frac{1}{4}\left\{\left(\frac{1}{c_s}\right)^2 - \left(\frac{1}{c_b}\right)^2\right\}^2 \omega^4\right]^{1/2}. \tag{2b}$$

In Eqs. (2a) and (2b), c_b, c_s, q are defined as

$$c_b = \sqrt{\frac{E}{\rho}}, \quad c_s = \sqrt{\frac{KG}{\rho}}, \quad q = \sqrt{\frac{I}{A}},$$

where Young's modulus, the shear modulus and density are denoted by E, G and ρ, respectively. The cross-sectional area and mass moment of inertia are expressed by A and I, and the value of shear correction factor K is taken to be 0.8.

For frequencies below 30 kHz, which we will be mainly interested in, k_H will be purely imaginary. Therefore, the wavenumber k will be $k(\omega) = k_L(\omega)$ for the propagating wave part $(e^{+ik_i x}, e^{-ik_i x})$, and $k(\omega) = |\mathrm{Im}\, k_H(\omega)|$ for the evanescent wave part $(e^{+k_i x}, e^{-k_i x})$. If necessary, the axial stress σ_x can be determined by the following equation:

$$\sigma_x = -Ey\frac{\partial\theta(x,t)}{\partial x}. \tag{3}$$

After some analysis, we can show that the following relation holds between the coefficients (A, B, C, D) and $(\bar{A}, \bar{B}, \bar{C}, \bar{D})$ of Eq. (1) [12]:

$$(GAK_1k^2)\begin{Bmatrix} A_i \\ B_i \\ C_i \\ D_i \end{Bmatrix} = (ikGAK_1)\begin{Bmatrix} \bar{A}_i \\ \bar{B}_i \\ \bar{C}_i \\ \bar{D}_i \end{Bmatrix} \quad (i = 1,2,3), \tag{4}$$

$$v_1 = v_2,$$

$$\phi_1 = \phi_2,$$

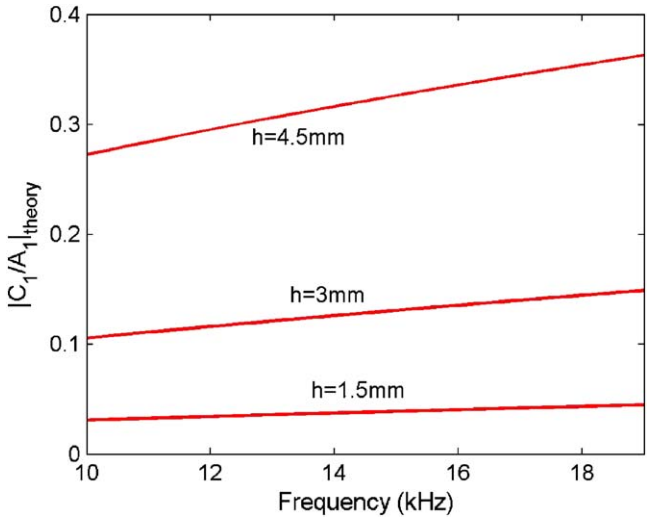

Fig. 3. The theoretical value of $|\bar{C}_1/\bar{A}_1|$ by the Timoshenko beam theory for varying values of the crack size h. (diameter $D = 10\,\text{mm}$, crack length $d = 2\,\text{mm}$).

$$E_1 I_1 \frac{\partial \phi_1}{\partial x} = E_2 I_2 \frac{\partial \phi_2}{\partial x},$$

$$-E_1 I_1 \frac{\partial^2 \phi_1}{\partial x^2} - \rho\omega^2 I_1 \phi_1 = -E_2 I_2 \frac{\partial^2 \phi_2}{\partial x^2} - \rho\omega^2 I_2 \phi_2. \tag{5}$$

At the crack boundaries, at $x = 0$ and $x = d$, the imposition of the displacement and force continuities yields the necessary equation to calculate the ratio $|\bar{C}_1/\bar{A}_1|$ in Eq. (5).

Fig. 3 shows the dependence of $|\bar{C}_1/\bar{A}_1|$ on the frequency for varying values of the crack size h. The ratio $|\bar{C}_1/\bar{A}_1|$ that is calculated theoretically by the Timoshenko beam theory will be denoted as $|\bar{C}_1/\bar{A}_1|_{\text{theory}}$. The frequency dependence of the ratio on the crack size will be used for the crack size estimation.

3. The measurement technique and experimental setup

3.1. The measurement principle of the magnetostrictive sensor

To measure bending waves in a beam, we use the magnetostrictive sensor. The principle of the sensor and its application may be found in Refs. [16,22,23]. The main motivation to use the magnetostrictive sensor is that stress waves can be measured without any direct physical contact. This non-contact characteristic of the sensor has been favored in many applications. The underlying principle of the magnetostrictive sensor is based on the Villari effect, which, in the one-dimension form, can be expressed as

$$B = \mu^{\sigma} H + q\sigma, \tag{6}$$

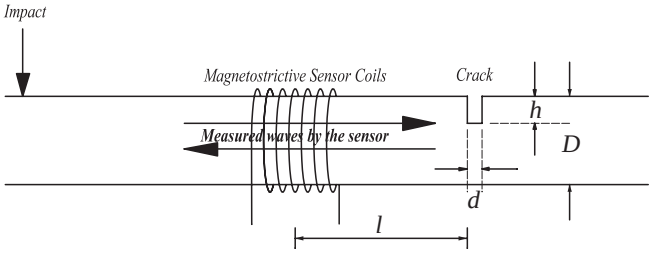

Fig. 4. The schematic diagram of the experimental setup.

where B and H denote magnetic induction and magnetic field strength, respectively. The stress is denoted by σ. Two coefficients μ^{σ} and q represent the permeability under constant stress and the Villari effect coefficient, respectively [23,24].

In our experiments, the solenoid coils of the magnetostrictive sensor encircle a circular beam (see Figs. 4 and 5). If stress is developed where the sensor coils encircle, the variation of the magnetic state caused by the stress can be measured through the sensor coil as the voltage change [22,25]:

$$V(x,t) = -\frac{\mathrm{d}\Phi}{\mathrm{d}t} = -N\,\frac{\mathrm{d}\phi}{\mathrm{d}t}, \tag{7}$$

where x is the longitudinal location along the beam axis and t denotes time. The symbol Φ denotes the total magnetic flux enclosed by the sensor coils and $V(x,t)$ represents the voltage output between both ends of the coils. The magnetic flux encircled by one turn of the coils is denoted by ϕ, and the number of the coil turns is N.

Since the magnetic flux is related to the magnetic induction, the output voltage can be written as

$$V(x,t) = -N\,\frac{\mathrm{d}}{\mathrm{d}t}\int_A B\,\mathrm{d}A, \tag{8}$$

where A denotes the cross-sectional area of the beam. Assuming that the applied magnetic field strength H is not time-varying, we can find the following equation from Eqs. (6) and (8):

$$V(x,t) = -N\,\frac{\partial}{\partial t}\int_A q\sigma\,\mathrm{d}A. \tag{9}$$

When bending waves propagate in a long slender beam, the stress distribution is given by Eq. (3). To measure bending waves effectively, the distribution of q about y should be the same as the stress distribution in Eq. (3). If non-linearity and hysteresis are ignored, the magnetostriction coefficient q can be expressed as

$$q(x,y) = c_0(x) + c_1(x)y + \cdots. \tag{10}$$

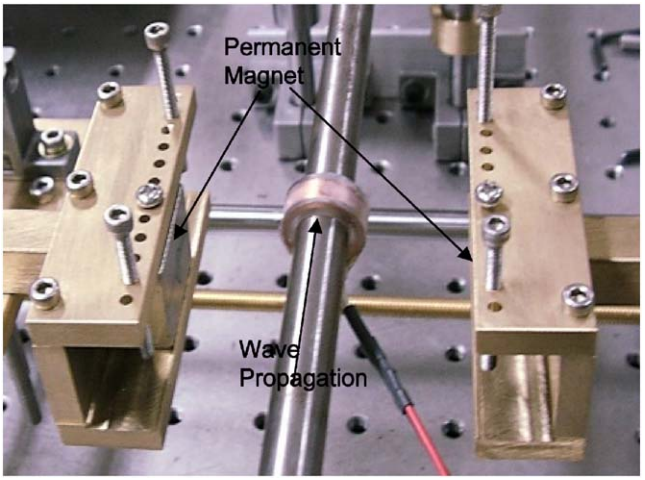

Fig. 5. The photo of the installed sensor consisting of the coils and the bias permanent magnets.

If the stress field is caused by bending and the two-term expression in Eq. (10) is used, the output voltage $V(t)$ measured by the sensor coils becomes [19]

$$V(x,t) \approx NEIc_1(x)\frac{\partial}{\partial t}\left(\frac{\partial \theta}{\partial x}\right) \equiv Q\frac{\partial}{\partial t}\left(\frac{\partial \theta}{\partial x}\right), \tag{11}$$

where $I = \int_A y^2 \, dA$ is the mass moment of inertia of the beam. In the last expression of Eq. (11), the dependence of Q on x is dropped as the sensing location will be assumed to remain unchanged during experiments.

3.2. Experimental arrangement

Fig. 4 shows how the magnetostrictive sensor is placed at the measurement point; the sensor coils will detect the change of the magnetic state induced by the stress wave in a beam cross section. The experimental configuration setup for a test beam specimen is shown in Fig. 5. Bending waves in the test beam were generated by the side impact of a small cylindrical bullet. The bullet was shot by an air gun system that was also used in Lee and Kim [21]. The bending waves were measured by the solenoidal coils of the magnetostrictive sensor.

The diameter and length of the cylindrical ferromagnetic beam used in this experiment were 10 and 2000 mm, respectively. For the present investigations, we considered three cracks having the depths $h = 1.5$, 3.0, and 4.5 mm for the beam in Fig. 1(a) and $h = 1.8$, 2.8, and 4.0 mm for the beam in Fig. 1(b). However, the width of crack was fixed as $d = 2$ mm.

Note that the permanent magnets in Fig. 5 should be arranged so as to make q vary linearly along the beam cross section. The magnet configuration employed in this work was suggested by Lee and Kim [21].

The voltage measured by the solenoid sensor was amplified by a preamplifier (Stanford Research Systems SR560) and captured by a digital oscilloscope (Lecroy 9310 M). The sampling rate was 20 Ms/s.

4. CWT ridge analysis for crack size estimation

In this section, we will present a technique to estimate $|\bar{C}_1/\bar{A}_1|$ by the continuous wavelet transform. The ratio $|\bar{C}_1/\bar{A}_1|$ is the magnitude of the reflected wave to the magnitude of the incident wave.

To motivate the need for the wavelet transform, we plot the measured signal consisting of the waves incident to and reflected from a crack ($d = 2$ mm, $h = 4.5$ mm) in Fig. 6. From the time signal shown in Fig. 6, it is impossible even to distinguish the incident part from the reflected part. Therefore, time–frequency analysis using the short-time Fourier transform, or the wavelet transform should be used for damage estimation. Recently, Kim and Kim [9] have shown that certain bending waves measured in a beam must be analyzed by the wavelet transform in order to extract the arrival time and the frequency component of the wave signals accurately. Accordingly, we use the continuous transform based on the Gabor wavelet [4]. After a brief introduction of the wavelet ridge analysis, we will show how the ridge analysis can be applied to the present beam bending problem.

4.1. Wavelet ridge analysis

Since wave signals to be measured are highly dispersive, the frequency components arriving at the measurement point vary rapidly in a short period. Our strategy to estimate $\bar{A}_1$ and $\bar{C}_1$ that are the frequency-dependent magnitudes of the incident and reflected waves, respectively, is to find the ridges in the time–frequency plane of the continuous wavelet transform and determine the magnitudes at the ridges.

Since the continuous Gabor wavelet transform will be employed, it is necessary to explain the continuous wavelet transform briefly. In analyzing the frequency evolution of a signal using

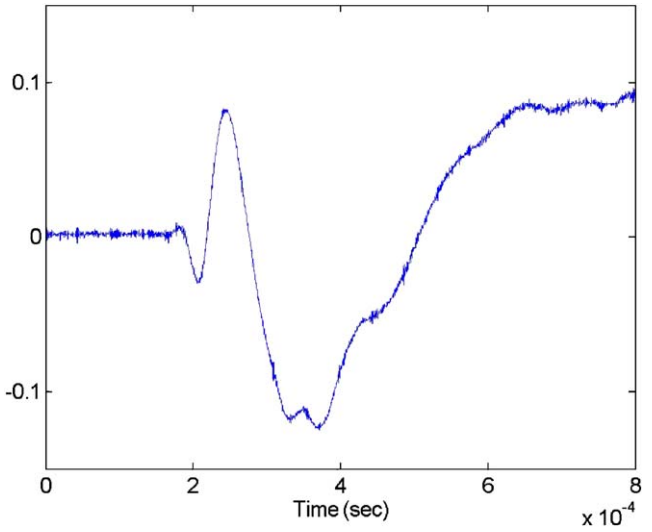

Fig. 6. The time history of the voltage signal measured by the magnetostrictive sensor in a cracked beam ($D = 10$ mm, $d = 2$ mm, $h = 4.5$ mm, $l = 150$ mm).

CWT, one must use analytic wavelets such as the Gabor wavelet that has the smallest Heisenberg box [4]. The Gabor wavelet is a complex-valued modulated Gaussian function, which is defined as

$$\psi(t) = g(t)\mathrm{e}^{\mathrm{i}\eta t}, \tag{12}$$

where the center frequency of the Fourier transforms $\hat{\psi}$ is η and $g(t)$ is a Gaussian function

$$g(t) = \frac{1}{(\sigma^2\pi)^{1/4}} \exp\left(\frac{-t^2}{2\sigma^2}\right). \tag{13}$$

It is pointed out in Ref. [9] that the time–frequency characteristics of the Gabor wavelet transform are controlled by the Gabor shaping factor $G_s = \sigma\eta$. In our applications, the value of $G_s = 3.5$ will be used and the validity of using this value will be checked later for the problem in consideration.

To explain the ridge analysis, we assume that a signal $V(t)$ to be analyzed takes the following form:

$$V(t) = a(t)\mathrm{e}^{\phi(t)}, \tag{14}$$

where $a(t)$ is called the analytic amplitude of $V(t)$ and $\phi(t)$ is the modulating phase. Then the wavelet transform $W_V(u,s)$ of $V(t)$ takes the following form:

$$\begin{aligned} W_V(u,s) &= \int_{-\infty}^{+\infty} V(t)\frac{1}{\sqrt{s}}\psi^*\left(\frac{t-u}{s}\right)\mathrm{d}t \\ &= \frac{\sqrt{s}}{2}a(u)\mathrm{e}^{\mathrm{i}\phi(u)}(\hat{g}(s[\xi-\phi'(u)]) + \varepsilon(u,\xi)) \end{aligned} \tag{15}$$

with

$$\psi_{u,s}(t) = \frac{1}{\sqrt{s}}\psi\left(\frac{t-u}{s}\right).$$

In Eq. (15), u and s denote the time and scale, and the symbol * denotes the complex conjugate.

The ridge algorithm computes the instantaneous frequencies from the local maxima of $|W_V(u,s)|$. If the following conditions are satisfied [9], the corrective term $\varepsilon(u,\xi)$ in Eq. (15) can be neglected and the use of Eq. (15) can be adjusted for our applications:[1]

$$\eta \ll \sqrt{\frac{|a(u)||\mathrm{d}\phi(u)/\mathrm{d}u|}{\mathrm{d}^2a/\mathrm{d}u^2}}, \tag{16a}$$

$$\eta \ll \frac{\|\mathrm{d}\phi(u)/\mathrm{d}u\|}{\sqrt{\mathrm{d}^2\phi/\mathrm{d}u^2}}, \tag{16b}$$

$$\eta \ll 1. \tag{16c}$$

In Fig. 7, the three conditions corresponding to Eqs. (16a–c) are plotted in the frequency range of interest (between 5 and 25 kHz). Since all of the three conditions are satisfied for $G_s = 3.5$, the CWT-based ridge analysis can be justified for the frequencies of interest.

[1]The suggestion of an anonymous reviewer to justify the use of Eq. (15) is appreciated.

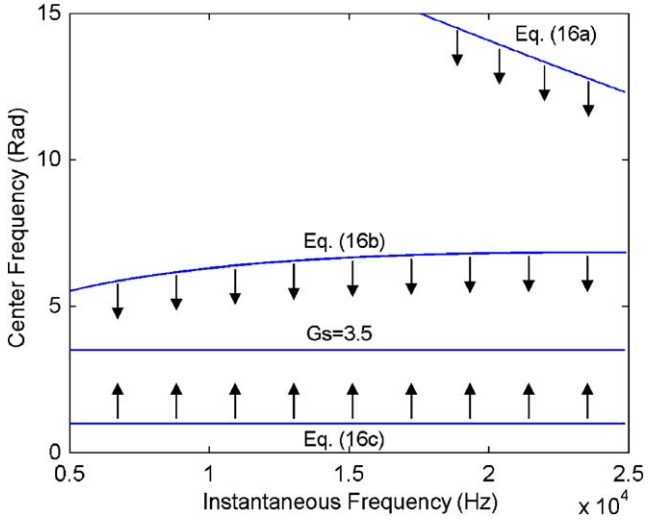

Fig. 7. The allowable range of the center frequency η for CWT for $G_s = 3.5$.

Since $|\hat{g}(\omega)|$ is maximum at $\omega = 0$, $|W_V(u,s)|$ becomes the maximum at $\xi = \phi'(u)$, where $\phi' = \mathrm{d}\phi/\mathrm{d}u$. The locus connecting the points (u,ξ) that locally maximize $|W_V(u,s)|$ is called the ridge. At the ridge point $(u,\xi(u))$, we have

$$|W_V(u,s)| = \frac{\sqrt{s}}{2}\,|a(u)||\hat{g}(o)| \tag{17a}$$

or

$$|a(u)| = 2|W_V(u,s)|/|\hat{g}(0)|. \tag{17b}$$

Therefore, $|a(u)|$, i.e., the magnitude of the signal along the ridge can be determined if $|W_V(u,s)|$ along the ridge is known.

In interpreting $W_V(u,s)$, it is often convenient to use the frequency ω instead of the scale s using the relation $s \approx \eta/\omega$ (η is the center frequency of the wavelet $\hat{\psi}$). Because there is no danger of confusion between u and t, we also use t instead of u as

$$\tilde{W}_V(t,\omega) = W_V(u,s). \tag{18}$$

4.2. Continuous Gabor wavelet transform application to bending problems

Now we will show how Eq. (17) is used to estimate $|\bar{C}_1/\bar{A}_1|$ from the measured signal. For the subsequent analysis, the wave mechanics is based on the Timoshenko beam theory that is summarized in Section 2. Since the measured sensor signal $V(t)$ in a cracked beam consists of the contributions $V_i(t)$ and $V_r(t)$ from both the incident wave and reflected wave, we write $V(t)$ as

$$V(t) = V_i(t) + V_r(t). \tag{19}$$

If the sensor location is not very close to either the impact point or the crack, one may neglect the contribution of the evanescent waves to the measured sensor output voltage $V(t)$ as they decay rapidly.

Using the Timoshenko bending wave model in Eqs. (1b) and (11) for the sensor output, $V_i(t)$ and $V_r(t)$ can be written as

$$\begin{aligned} V_i(t) &= Q\frac{\partial}{\partial t}\frac{\partial}{\partial x}\left(\bar{A}_1 e^{i(-k_1 x+\omega t)}\right) \\ &= Q\bar{A}_1 k_1 \omega e^{i(-k_1 x+\omega t)}, \end{aligned} \tag{20a}$$

$$\begin{aligned} V_r(t) &= Q\frac{\partial}{\partial t}\frac{\partial}{\partial x}\left(\bar{C}_1 e^{i(k_1 x+\omega t)}\right) \\ &= -Q\bar{C}_1 k_1 \omega e^{i(k_1 x+\omega t)}. \end{aligned} \tag{20b}$$

Comparing Eqs. (14) and (20), the analytic amplitudes $a_i(t)$ and $a_r(t)$ of the incident and reflected parts of the measured signal become

$$a_i(t) = Qk_1\omega e^{-ik_1 x}\bar{A}_1, \tag{21a}$$

$$a_r(t) = -Qk_1\omega e^{ik_1 x}\bar{C}_1. \tag{21b}$$

Now using Eqs. (17a), (18) and (21), we obtain

$$\begin{aligned} \frac{|\tilde{W}_{V_r}(t,\omega)|_{\text{ridge}}}{|\tilde{W}_{V_i}(t,\omega)|_{\text{ridge}}} &= \frac{\sqrt{\eta/\omega}/2\cdot|a_r||\hat{g}(0)|}{\sqrt{\eta/\omega}/2\cdot|a_i||\hat{g}(0)|} \\ &\approx \frac{|Qk_1\omega e^{-ik_1 x}|}{|-Qk_1\omega e^{ik_1 x}|}\frac{|\bar{C}_1|}{|\bar{A}_1|} \\ &= \left|\frac{\bar{C}_1}{\bar{A}_1}\right|. \end{aligned} \tag{22}$$

Therefore, if we determine the magnitudes of $|\tilde{W}_{V_r}(t,\omega)|$ and $|\tilde{W}_{V_i}(t,\omega)|$ along their ridges, the ratios of $|\bar{C}_1/\bar{A}_1|$ can be estimated. Since the ratio depends on the damage size, we can extract the damage size for which the experimentally determined ratio $|\bar{C}_1/\bar{A}_1|_{\text{exp}}$ fits best the theoretical ratio $|\bar{C}_1/\bar{A}_1|_{\text{theory}}$ by the Timoshenko beam theory.

Thus, the estimated depth h_{est} is computed by

$$h_{\text{est}} = \arg\min_h \sum_\omega \left[\left|\frac{\bar{C}_1(\omega)}{\bar{A}_1(\omega)}\right|_{\text{exp}} - \left|\frac{\bar{C}_1(\omega;h)}{\bar{A}_1(\omega;h)}\right|_{\text{theory}}\right]^2. \tag{23}$$

Because $|\bar{C}_1(\omega)/\bar{A}_1(\omega)|$ is frequency dependent, we look for h_{est} that minimizes the difference between $|\bar{C}_1(\omega)/\bar{A}_1(\omega)|_{\text{exp}}$ and $|\bar{C}_1(\omega)/\bar{A}_1(\omega)|_{\text{theory}}$ over a certain frequency range.

5. Applications

In this section, we will present the results obtained by the CWT ridge technique for the estimation of $|\bar{C}_1/\bar{A}_1|_{\text{exp}}$. As an example, we take the continuous Gabor wavelet transform of the voltage signal $V(t)$ of Fig. 6 and plot $|\tilde{W}_V(t,\omega)|$ in Fig. 8. (The value of $G_s = 3.5$ for CWT was used.) From the three-dimensional plot alone, it is still difficult to tell which part of the plot corresponds to the incident part (V_i) or the reflected part (V_r). Therefore, the contour of $|\tilde{W}_V(t,\omega)|$ in the time–frequency plane was used. To find the ridges, we searched for the loci of the local maxima of $|\tilde{W}_V(t,\omega)|$.

Before applying CWT, the noise removal of measured signals was done. (We used the function "wden" of Matlab.) The loci are marked in Fig. 9. The patterns of the loci clearly reveal the dispersive characteristics of the first branch (corresponding to $k = k_L(\omega)$) of the bending waves. It is difficult to pinpoint the reflected wave part from the direct time signal in Fig. 6, but the ridge analysis shows the arrival of the wave reflected from the crack. Once the ridges for the incident and reflected waves are determined, one can find the magnitudes of $|\tilde{W}_{V_i}(t(\omega),\omega)|_{\text{ridge}}$ and $|\tilde{W}_{V_r}(t(\omega),\omega)|_{\text{ridge}}$.

Now using Eq. (22), we can estimate the ratios $|\bar{C}_1/\bar{A}_1|$ and plot them in Fig. 10 for various values of h's. The experimental results in Fig. 10 clearly indicate that the magnitude and the frequency-dependence characteristic of $|\bar{C}_1/\bar{A}_1|$ vary depending on the values of h's for the beam in Fig. 1(a).

To estimate h's from $|\bar{C}_1/\bar{A}_1|_{\text{exp}}$, Eq. (23) was used. The results for three cases ($h = 1.5$, 3.0, 4.5 mm) for the beam in Fig. 1(a) are summarized in Table 1. It is worth comparing the frequency dependencies of $|\bar{C}_1/\bar{A}_1|_{\text{theory}}$ and $|\bar{C}_1/\bar{A}_1|_{\text{exp}}$ and the comparison is shown in Fig. 11. The analysis used for the beam in Fig. 1(a) was repeated for the beam in Fig. 1(b). The results are given by Table 2 and Fig. 12.

When the damage size becomes large, the estimated crack size approaches the true values of h's. A relatively large discrepancy between h_{true} and $h_{\text{estimated}}$ mostly for small values of h's may be

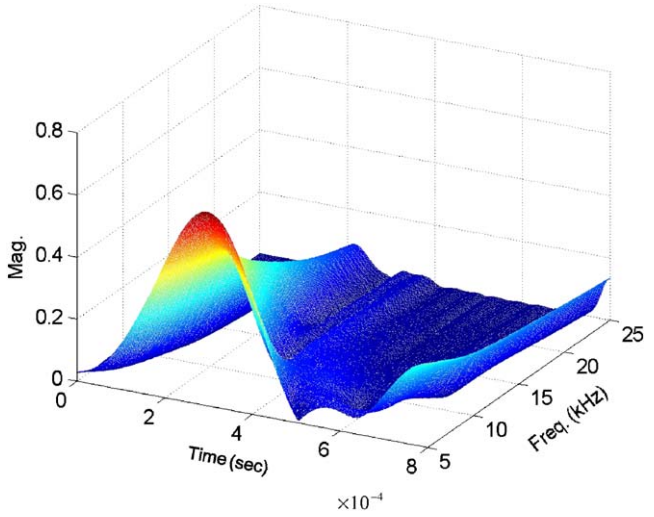

Fig. 8. The three-dimensional plot of $|\tilde{W}_V(t,\omega)|$ of the signal shown in Fig. 6.

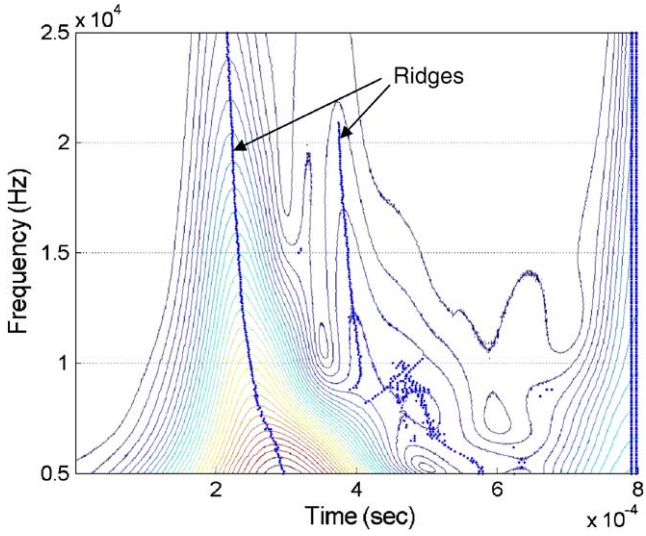

Fig. 9. The ridges of $|\tilde{W}_V(t,\omega)|$ plotted on the two-dimensional contour plot. (The signal $V(t)$ is from Fig. 6.)

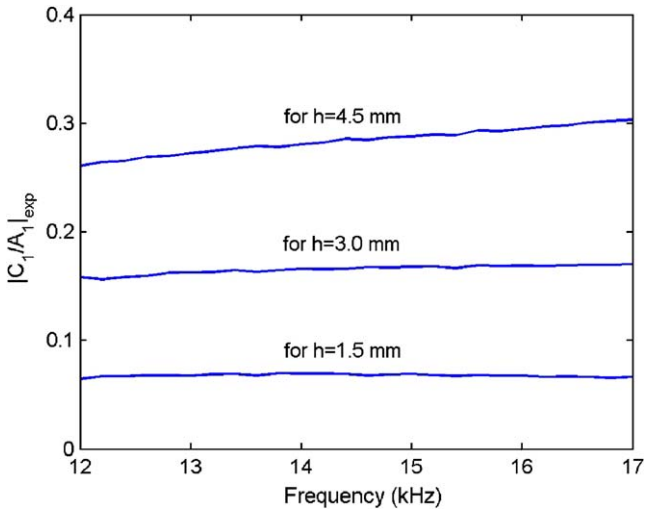

Fig. 10. The estimated ratios $|\tilde{C}_1/\tilde{A}_1|_{\exp}$ from the wavelet ridge analysis for the experimentally measured signals.

Table 1
Damage size estimation for the beam shown in Fig. 1(a)

Given (mm)	Estimated (mm)	Error
1.5	2.2	0.46
3.0	3.4	0.13
4.5	4.3	0.04

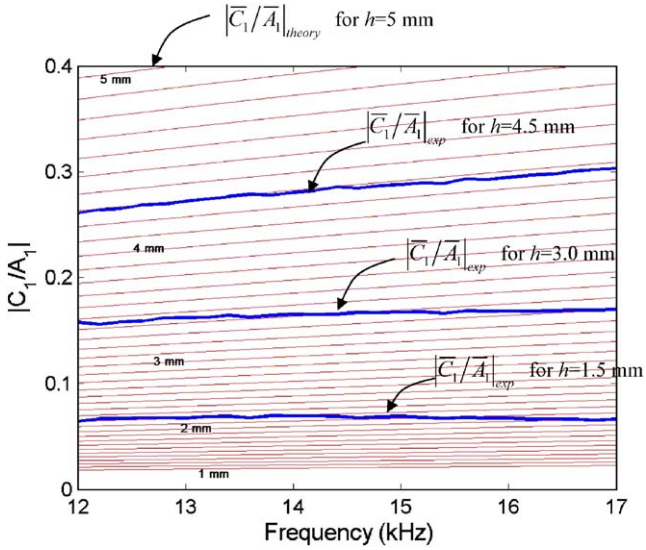

Fig. 11. The comparison of $|\bar{C}_1/\bar{A}_1|_{\text{theory}}$ and $|\bar{C}_1/\bar{A}_1|_{\text{exp}}$ in a partial-cracked beam.

Table 2
Damage size estimation of the beam shown in Fig. 1(b)

Given (mm)	Estimated (mm)	Error
1.8	1.6	0.11
2.8	3.0	0.07
4.0	3.7	0.08

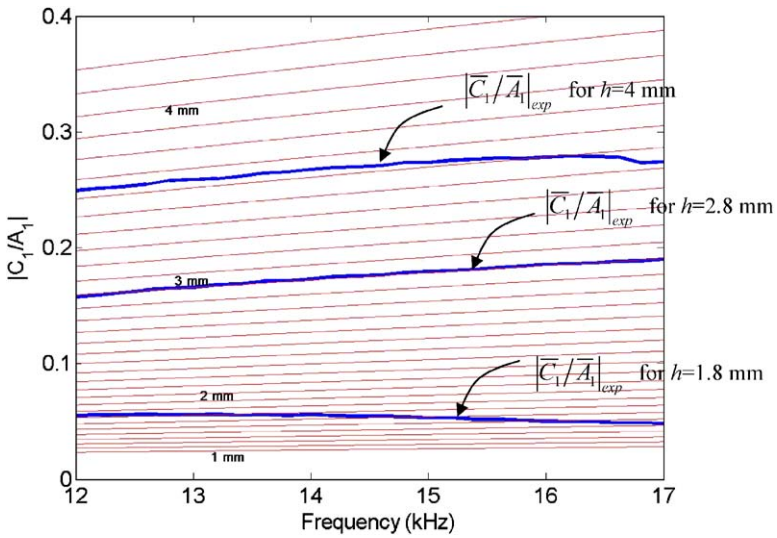

Fig. 12. The comparison of $|\bar{C}_1/\bar{A}_1|_{\text{theory}}$ and $|\bar{C}_1/\bar{A}_1|_{\text{exp}}$ in a circumferential-cracked beam.

from several sources. The major source appears to come from the incapability of the Timoshenko beam theory to predict the wave phenomena for small cracks. In order to improve the estimation accuracy, among others, the three-dimensional elasticity solution should be used.

6. Conclusions

The continuous Gabor wavelet transform was used to estimate the damage size from dispersive bending waves in a beam. In the time–frequency plane of the continuous wavelet transform, the magnitudes of the wavelet transform along the ridges of the incident and reflected waves are used for the damage size estimation. We showed that the ratio of these magnitudes along the two ridges is the same as the ratio of the magnitude of the incident wave to the magnitude of the reflected wave. By using the fact that the magnitude and frequency-dependence pattern of the ratio vary with damage size, we were able to correlate the ratio and the damage size. Except when the damage size is very small, which would require the use of advanced theories, the correlation was quite satisfactory.

References

[1] E. Bray, R.K. Stanley, *Nondestructive Evaluation*, CRC Press, New York, 1997.
[2] M.J. Mcgonnagle, *Nondestructive Testing*, Gordon and Breach, New York, 1961.
[3] Y.Y. Kim, E.H. Kim, A new damage detection method based on a wavelet transform, in: *Proceedings of 18th IMAC*, 2000, pp. 1207–1212.
[4] S. Mallat, *A Wavelet Tour of Signal Processing*, Academic Press, London, 1998.
[5] J. Slavic, I. Simonovski, M. Boltezar, Damping identification using a continuous wavelet transform: application to real data, *Journal of Sound and Vibration* 262 (2003) 291–307.
[6] H. Inoue, K. Kishimoto, T. Shibuya, Experimental wavelet analysis of flexural waves in beams, *Experimental Mechanics* 36 (1996) 212–217.
[7] K. Kishimoto, H. Inoue, M. Hamada, T. Shibuya, Time–frequency analysis of dispersive waves by means of wavelet transform, *Journal of Applied Mechanics* 62 (1995) 841–846.
[8] T. Onsay, A.G. Haddow, Wavelet transform analysis of transient wave propagation in a dispersive medium, *Journal of the Acoustical Society of America* 95 (1994) 1441–1449.
[9] Y.Y. Kim, E.H. Kim, Effectiveness of the continuous wavelet transform in the analysis of some dispersive elastic waves, *Journal of the Acoustical Society of America* 110 (2001) 86–94.
[10] W.J. Staszewski, Identification of non-linear systems using multi-scale ridges and skeletons of the wavelet transform, *Journal of Sound and Vibration* 214 (1998) 639–658.
[11] W. Weaver, S.P. Timoshenko, D.H. Young, *Vibration Problems in Engineering*, Wiley, New York, 1990.
[12] J.F. Doyle, *Wave Propagation in Structures*, second ed., Springer, New York, 1997.
[13] J.D. Achenbach, *Wave Propagation in Elastic Solids*, North-Holland, New York, 1973.
[14] H. Kwun, K.A. Bartel, Experimental observation of elastic-wave dispersion in bounded solids of various configuration, *Journal of the Acoustical Society of America* 99 (1996) 962–968.
[15] H. Kwun, K.A. Bartel, Experimental observation of wave dispersion in cylinder shell via time–frequency analysis, *Journal of the Acoustical Society of America* 97 (1995) 3905–3907.
[16] H. Kwun, K.A. Bartel, Magnetostrictive sensor technology and its application, *Ultrasonics* 36 (1998) 171–178.
[17] H. Kwun, C.M. Teller, Magnetostrictive generation and detection of longitudinal, torsional, and flexural waves in a rod, *Journal of the Acoustical Society of America* 96 (1994) 1202–1204.

[18] J.C. Aime, M. Brissaud, L. Laguerre, Spatial analysis of torsional wave propagation in a cylindrical waveguide. Application to magnetostrictive generation, *Journal of the Acoustical Society of America* 109 (2001) 51–58.
[19] Y.Y. Kim, S.H. Cho, H. Lee, Application of magnetomechanical sensors in modal testing, *Journal of Sound and Vibration* 268 (2003) 799–808.
[20] H. Lee, Design and Analysis of a Mode Selectable Stress Wave Sensor using the Villari Effect, Ph.D. Thesis, Seoul National University, 2001.
[21] H.C. Lee, Y.Y. Kim, Wave selection using a magnetomechanical sensor in a solid cylinder, *Journal of the Acoustical Society of America* 112 (2002) 953–960.
[22] R.C. Williams, Theory of magnetostrictive delay lines for pulse and continuous wave transmission, *IEEE Transactions on Ultrasonic Engineering* 7 (1959) 16–38.
[23] D.C. Jiles, Theory of magnetomechanical effect, *Journal of Physics D: Applied Physics* 28 (1995) 1537–1546.
[24] D. Jiles, *Introduction to Magnetism and Magnetic Materials*, Chapman & Hall, London, 1991.
[25] M. Onoe, Theory of ultrasonic delay lines for direct-current pulse transmission, *Journal of the Acoustical Society of America* 34 (1962) 1247–1254.